SEPARATION AND TRAPPING OF MICROPARTICLES UTILIZING AC ELECTROOSMOTIC FLOW IN A Y-SHAPED MICROCHANNEL WITH ASYMMETRIC ELECTRODE PAIRS

KAO-FENG YARN, YU-JEN PAN[a], WIN-JET LUO[b*], CHUN-NAN CHEN[c]
Department of Electronic Engineering, Far East University, Tainan 744, Taiwan
[a]Department of Computer and Communications Engineering, Ta Hwa Institute of Technology, Hsinchu 307, Taiwan
[b]Department of Refrigeration, Air-Conditioning and Energy Engineering, National Chin-Yi University of Technology, Taichung City 411, Taiwan
[c]Department of Physics, Tamkang University, New Taipei City, Taiwan

In this study, for clearer inspection of biosamples, a Y-shaped microchannel with a downstream sudden expansion channel in which a series of asymmetric microelectrode pairs were embedded was designed to separate and trap the microparticles within NaCl (sodium chloride) liquid. NaCl liquid, with different sized particles, was injected through one inlet of the Y-shaped microchannel. In the pinched segment of the channel, the injected particles were pinched by another NaCl liquid introduced through another inlet of the Y-shaped microchannel and aligned along a sidewall. AC electric potentials were applied to each pair of asymmetric electrodes, generating a non-uniform electrical field resulting in small and large rolls on the electrodes. While the small particles passed through the electrodes, the particles were introduced into the rolls and trapped within the pairs of electrodes. Through the specific Y-shaped microchannel and the induced AC electroosmotic flow within the sudden expansion microchannel, separation and trapping of microparticles can be achieved continuously and simultaneously.

1. Introduction

In order to deal with biosamples, many methods and developed techniques are applied to separate the necessary samples, extract the material within cells and process sample inspection. Accurate inspection results can be provided through conventional detection of microorganisms. However, the procedures take a lot of time and expense. To develop a fast and accurate detection system is an important issue in the diagnosis of pathogens. Developing separation techniques include: field flow fractionation (FFF) [1-4], hydrodynamic chromatography (HDC) [5-8], capillary hydrodynamic fractionation (CHDF) [9-11] and split-flow thin (SPLITT) fractionation [12-15]. As mentioned above, these methods have their advantages and drawbacks. The technologies of FFF, HDC and CHDF mainly employ flow distribution to separate microparticles in microchannels or in capillaries. Additional effects, including gravitational force, centrifugal force, electrical field and heat, are necessary for FFF technology to enhance particle separation efficiency. For the technologies of CHDF and HDC, additional effects are unnecessary during the particle separation procedure. The separation efficiencies of the abovementioned approaches are very high, but take a long time for the separation procedures to finish.

Separation of different sized particles and the measurement of particle sizes remain important issues in industrial production, environmental evaluation and biochemical study. These particles can be macromolecule particles, cells and pharmaceutical latex. Especially particles and cells are often manipulated within microfluidic chips during biochemical analysis, and need to be detected by optics [16-17]. Effective manipulation of particles or cells in the microchannels can promote reaction analysis processes on microfluidic chips and can also shorten the inspection time or space required during biochemical analysis. In order to obtain better efficiency in optical detection, especially in the inspection process, it is necessary to effectively manipulate particles to avoid too many particles or cells from passing through the optical detection zone at the same time, which could seriously affect accuracy.

In the relevant studies, Fu et al. [18] developed a disposable microfabricated fluorescence-activated cell sorter (μFACS) for sorting various biological entities. This sorter can result in substantial enrichment of micron-sized fluorescent bead populations of differing colors. The study separated Escherichia coli cells expressing green fluorescent protein from a background of non-fluorescent E. coli cells and showed that the bacteria are viable after extraction from the sorting device. Plenert and Shear [19] used capillary electrophoresis (CE) to separate the cells in order to enhance the efficiency of optic detection. Yamada et al. [20] developed a method of "pinched flow fractionation" for the continuous size separation and analysis of particles in microfabricated devices. This method utilizes only the laminar flow profile inside a microchannel, allowing elimination of complicated outer field control which is usually required for other kinds of particle separation methods, such as field flow fractionation. Xuan et al. [21] experimentally investigated the near-wall electrophoretic motion of spherical particles in cylindrical capillaries. They found that same-sized particles move faster in smaller capillaries. This wall-enhancing effect becomes more significant when the size difference between the particle and capillary becomes smaller and when a dilute electrolyte solution (i.e., thicker electric double layer) is used. Xuan et al. [22-23] visualized the accelerated particle electrophoretic motions in converging-diverging microchannels on poly-(dimethylsiloxane) chips. They found the ratio of the particle velocity in the throat compared to that in the straight channel decreased when particles moved closer to either sidewall, and that the particle velocity ratio increased when particles moved slower. Kang et al. [24] used DC-dielectrophoresis (DC-DEP) to induce the motion of the dielectric particles in a spatially non-uniform DC electric field, and to separate the biological cells by size. The DC-DEP force acting on the cells at the corners of the hurdle is proportional to the cells' size. Thus, the moving cells deviate from the streamlines, and the degree of deviation is dependent on the cell size. In this paper, using this method, it was demonstrated that combined with the electroosmotic flow, mixed biological cells of a few to tens of micrometers difference in diameter can be continuously separated into different collecting wells. Chow and Du [25] fabricated a DEP-based microfluidic channel to trap water bacteria. The separation between the polystyrene bead and bacteria can be easily achieved with an appropriate operating frequency. Zhang and Koplik [26] used molecular dynamics simulations to investigate trajectory deflection and particle trapping in flows of nanoparticle suspensions past patterned surfaces. They indicated that patterned surfaces deflect particle trajectories to a degree dependent on their size and may be used as a vector chromatography separation technique. Khoshmanesh et al. [27] presented a microfluidic system which utilized a combination of dielectrophoretic (DEP) and hydrodynamic drag forces to separate Lactobacillus bacteria from a background of yeasts. Yamada et al. [28] presented an improved microfluidic device that enables hydrodynamic particle concentration and size-dependent separation to be carried out in a continuous manner; a device having a microchannel with one inlet and five outlets was designed and fabricated. By simply introducing particle suspension into the device, concentrations of 2.1-3.0 μm particles were increased 60-80-fold and were collected independently from each outlet.

2. Numerical and Experimental Methodology

2.1 Principle of AC electroosmotic flow and the designed device

When an AC electrical field is applied to electrodes, an electric current is established in the solution; this leads to the formation of a transient excess charge in the electric double layer. The surface of micro-electrodes will attract counter-ions to accumulate on the electrode surfaces,

as shown in Fig. 1. Negative ions are attracted to the electrode connected to the anode, and positive ions are attracted to the electrode connected to the cathode. In the figure, the dotted line and the arrow indicate equal electrical potential distribution and the electric field direction from the cathode electrode to anode electrode, respectively, and the full line indicates the direction of the induced electroosmotic flow. The components of the electrical potential normal to the electrode surface induce the charge in the double layer, while the tangential component (E_x) produces a body force (F_c) on the induced charge, thus moving the fluid in two rolls over the electrodes. The generated velocity field has a steady-state component which can be observed experimentally. In a symmetrical electrode array, the global average fluid motion is zero. To achieve unidirectional fluid movement, the electrode array is made non-symmetric, as shown in Fig. 1. This asymmetry leads to fluid rolls of different sizes over each electrode, leading in turn to a net fluid flow.
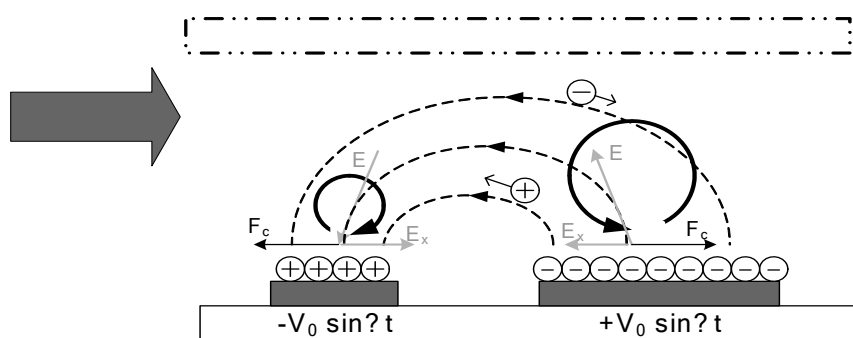

Fig.1. Induced flow field due to interaction of induced charges on electrodes and the applied AC electric field.

Green et al. [29-31] investigated the induced electrokinetic phenomenon on the planar electrodes in microchannels under the influence of AC electric fields. First, they experimentally detected an induced flow phenomenon above the electrodes and analyzed its velocity distributions. Then, they established physical modeling of the charged electric double layer above the electrodes in order to investigate the physical mechanism while the electrodes were charged by the applied AC electric fields. Finally, they simulated the whole induced AC electroosmotic flow within the microchannel.

In this study, a Y-shaped microchannel with a sudden downstream expansion channel in which asymmetric pairs of microelectrodes are embedded was designed to separate and trap the microparticles, as shown in Fig. 2. The NaCl liquid, with different sized particles injected through one inlet of the Y-shaped microchannel, is pinched at the joint segment of the channel by another NaCl liquid introduced from the other inlet of the Y-shaped microchannel. Thus, the particles are aligned to one sidewall of the joint channel in order to avoid two or more particles moving in two or more lines side-by-side. Then, the aligning particles enter the sudden expansion channel. Due to the centrifugal effect, the smaller particles are dragged forward along the streamline close to the sidewall of the expansion channel. However, the larger particles move along the streamline farther away from the sidewall. Through this process, the different sized particles moving along their corresponding specific streamline can be separated. In the expansion channel, a series of asymmetric microelectrode pairs are embedded in the region where the corresponding streamline of the smaller particles pass through on the glass substrate. When the AC electric potentials are applied to the electrodes, the smaller particles moving along the corresponding streamline are attracted to move into the induced rolls above the electrodes and are trapped between the electrode pairs, as shown in Fig. 2.
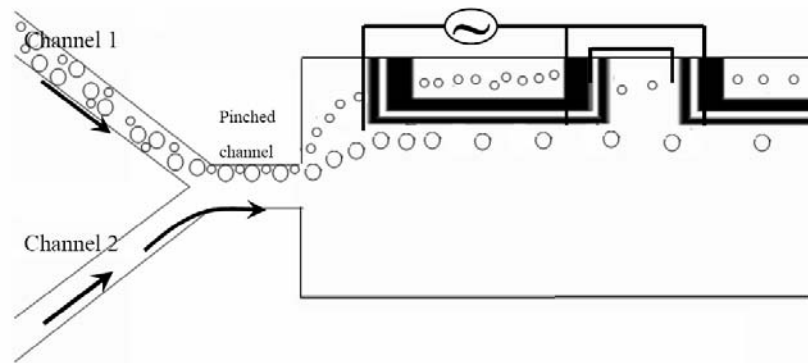
Fig. 2. Principle of the designed microdevice.

2.2 Numerical simulation

In this study, the software of CFD-ACE+, which is based on the finite volume method and is commercially available, is employed for simulating the flow field in a microchannel. In our calculations, we assume the fluid is Newtonian fluid and is an incompressible fluid. The effect of the body force on the particles is also ignored. There is no heat energy loss and exchange during the process. The fluid has a uniform diffusion constant and viscosity.

The working fluid used in this study is pure water ($\mu= 10^{-3}$ kg m^{-1} s^{-1}, ρ=1000 kg m^{-3}). The flow rate (R_1) of the fluid accompanied with different sized particles injected into one inlet channel is 1μl/h, and the flow velocity (R_2) of the fluid introduced from the other inlet channel is 7μl/h, respectively. The boundary condition at the inlets is set at a constant velocity value and the pressure value is set as zero. The boundary condition at the outlet is set with a pressure value of zero. A no-slip boundary condition is applied to the walls of the microchannel. The particles injected from one of the inlets move along the streamline of the flow and out through the outlet. When the moving particles collide with the walls, full reflection movement of the particles is assumed.

Governing equations are used in the numerical simulation, including: the conservation of mass equation (Eq. (1)), momentum equation (Eq. (2)), particle movement equation (Eq. (3)) and drag coefficient equation (Eq. (4)).

Conservation of mass:

$$\nabla \cdot \vec{V} = 0 , \tag{1}$$

where $\vec{V}$ represents the vector of the fluid velocity.

Momentum equation:

$$\rho \frac{D\vec{V}}{Dt} = -\nabla P + \mu \nabla^2 \vec{V} , \tag{2}$$

where ρ is the fluid density, P is the pressure and μ is the fluid viscosity.

Particle movement equation:

$$md\frac{du}{dt} = C_D \rho (U-u)|U-u|\frac{A_d}{2} + mdg + Sm, \tag{3}$$

where md is the mass of a particle, d is the particle's diameter, U is the surrounding flow field velocity of the particles and u is the velocity of the particles. A_d is the particle cross-sectional area and ρ is the fluid density.

$$\text{Drag coefficient:} \quad C_D = \frac{24}{\text{Re}} , \tag{4}$$

where $\text{Re} = \dfrac{\rho VD}{\mu}$ is the Reynolds number.

2.3 The fabrication of the PDMS channels

Soft lithography is a diverse set of techniques that encompasses replica molding, using an elastomeric material, specifically polydimethylsiloxane (PDMS), for the fabrication of microfluidic devices as well as for the patterning of surfaces using PDMS stamps (microcontact printing). The common procedure used for making PDMS channels involves the fabrication of a silicon master with patterned features composed of a photoresist (SU-8). In this process, silicon wafers were coated with a photoresist and then exposed to ultraviolet (UV) light through a mask with the desired pattern. High-resolution transparencies were used as the photomask to rapidly prototype SU-8 patterned masters, from which PDMS molds can be replicated. In the fabrication process, a silicone elastomer and elastomer curing agent (Sil-More Industrial Ltd, USA, Sylgard 184A and Sylgard 184B) were mixed in a ratio of 10:1 and then poured onto an SU-8 mold. The interrelated fabrication process refers to the work by Luo [32, 34]. The PDMS was cured at a temperature of 70°C for 1 h and then treated using oxygen plasma to change its inherent hydrophobic surface property to a hydrophilic property. The PDMS inverse structure was then peeled off the template.

To fabricate the microelectrodes, we use sodium glass as the substrate. This experimental wash also adopts RCA to wash the process in fabrication. It mainly washes particles off the glass surface, and then a photoresist is coated on the surface. HMDS is coated on the chip surface. This bonding effect is enhanced between the photoresist and glass chip. AZ4620 Positive photoresist 7μm is coated on a glass chip, and then sent into a furnace for a soft bake for 180 sec. By exposure with a UV lamp, the figure of the mask is moved to the chips as needed, using the mask to determine the required microelectrodes' figure from the photoresist. This thermally evaporates the microelectrodes on the glass surface. Most metal is evaporated by photoresist at this time, and then, some metal is evaporated on the glass surface. After the metal evaporates, the chip is immersed in acetone and put into an ultrasonic oscillator. By oscillation, the metal that remains after photoresist will be forced off. The residual metal on the glass surface is our designed microelectrode.

PDMS is viscoelastic. It acts like a viscous liquid, similar to honey. After polymerization and cross-linking, solid PDMS samples will present themselves on an external hydrophobic surface. This surface will appear metallic and shiny, although the substrate is clear. Its surface chemistry makes it difficult for polar solvents (such as water) to wet the PDMS surface and may lead to adsorption of hydrophobic contaminants. If PDMS combines with the sodium glass that evaporates with the metal, the surface quality must be changed by an oxygen-plasma operator. Finally, we combine the two materials together completing the designed microchip.

3. Results and discussion

The geometry of the designed particle trap and separation micro-device without the embedding of microelectrodes on the substrate is shown in Fig. 3. In the Y-shaped channel, the diameters of the reservoir at Inlet 1 and Inlet 2 are 200 μm. The lengths from Inlet 1 and Inlet 2 to the joint segment are both 5500 μm. The joint of Inlet 1's channel and Inlet 2's channel is a pinched segment 100 μm in length and 47 μm in width. The pinched segment connects a rectangular sudden expansion micro-channel in the downstream. The width of the sudden expansion micro-channel is 1000 μm, and the length is 1 cm, as shown in Fig. 3(a). A partial enlarged view is shown in Fig. 3(b). A squirm pump was used to inject the NaCl solution containing 5 μm and 15 μm of particles into Inlet Channel 1 with a flow rate of 1 μl/h, and the NaCl solution without particles was injected into Inlet Channel 2 with a flow rate of 7 μl/h, respectively. In order to allow the particles to align to one sidewall of the pinched channel, the width of the injected solution from Channel 1 in the pinched channel should be kept at 6.7 μm which is a little greater than 5 μm but less than 10 μm. While the width of the solution is maintained, two or more particles moving in two or more streamlines side-by-side can be avoided. That is the purpose of applying different and specific injecting flow rates in Channels 1 and 2. Each particle in the pinched channel will move along its corresponding stream line into the expansion microchannel. Figure 4 shows the calculated distributions of the streamlines in the Y-shaped microchannel. The corresponding streamlines of the particles of 5 μm and 15 μm are 937 μm and 829 μm from the bottom side of the expansion channel, respectively. The distance between the two corresponding streamlines is approximately 108 μm. According to Yamada et al. [16], the

calculation of the particle separation at the sudden expansion microchannel is shown as Eq. (5).

$$Y = (w_p - \frac{D_p}{2})\frac{W_B}{W_P},$$

(5)

where W_P and W_B are widths of the pinched segment and expansion microchannel, respectively. D_P is the diameter of the particle. The location of the 5 μm particles in the expansion channel is at 946.8 μm, and the location of the 15 μm particles is at 840.4 μm. The origin of the Y-axis and X-axis is located at the bottom corner of the sudden expansion channel. The distance between these two different sized particles is approximately 106.4 μm.
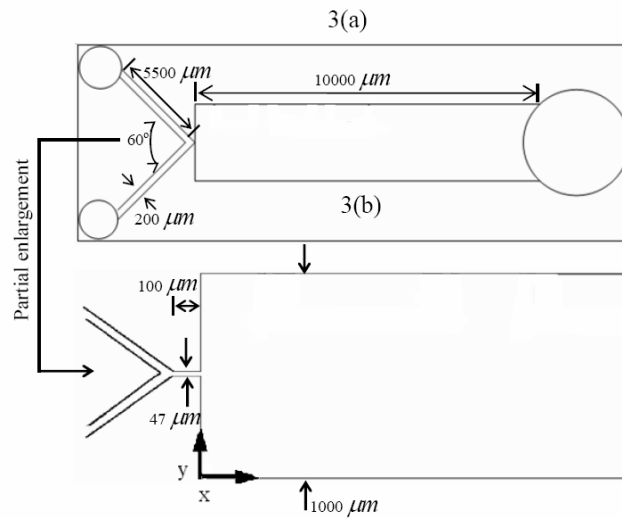
Fig. 3. Geometry of the particle separation device without microelectrodes.
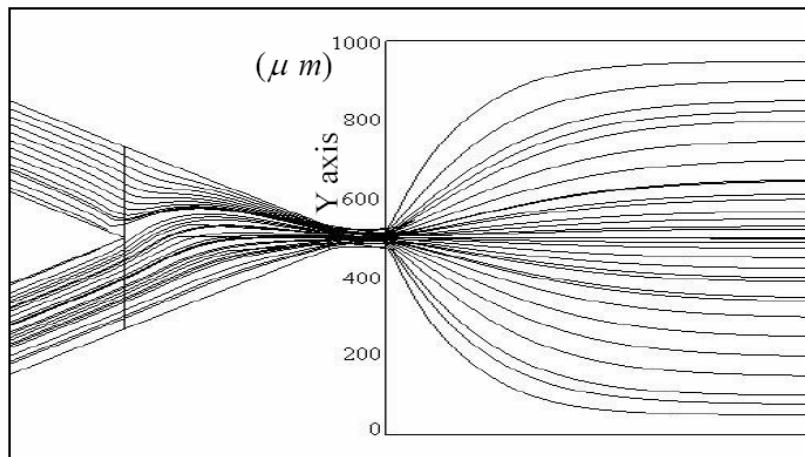
Fig.4. Streamline distribution in the microchannel.

Fig. 5 illustrates the distribution of fluorescent dye in the Y-shaped microchannel, released from Inlet 1 and flowing downstream with the solution injected at Inlet 1. The fluorescent dye in the pinched channel is distributed close to the upper sidewall of the channel, and the width of the fluorescent dye in the pinched channel becomes 6.7 μm. However, in the expansion channel, all of the fluorescent dye is distributed in the region within the U-shaped electrodes. Therefore, from the fluorescent dye distributions, we can ensure that the injected solution with particles can flow through the region of electrode pairs.
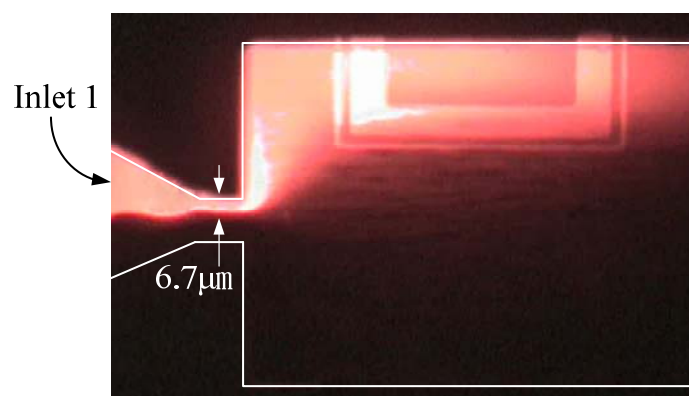
Fig. 5. Distribution of fluorescent dyes within the microchannel with microelectrodes.

Fig. 6 illustrates the moving trajectory of the 5 µm and 15 µm particles within the expansion channel. When the particles enter the sudden expansion microchannel, the distance between two particles gradually is enlarged with the downstream separation of the streamlines. Therefore, the trajectory of the smaller particle is closer to the sidewall, and its downstream location from the bottom sidewall is approximately 950 µm. However, the trajectory of the bigger particle is far from the sidewall, and its downstream location from the bottom sidewall is approximately 830 µm. The distance between the two different sized particles is approximately 120 µm. As shown in Fig. 6, after particles entered the sudden expansion microchannel, different sizes of particles moved downstream and separated.
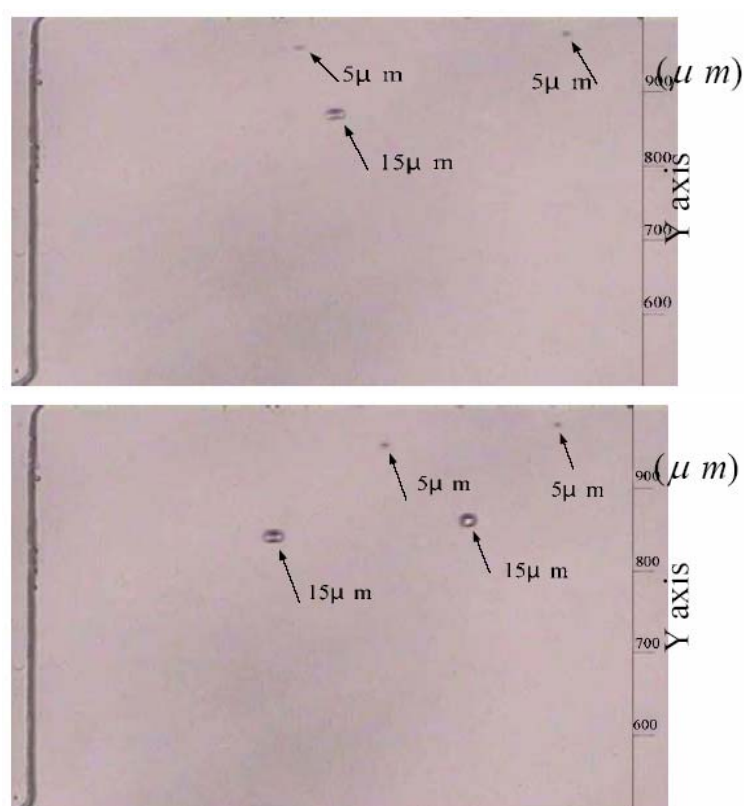

Fig. 6. Locations of particles with different sizes at the Y-axis in the sudden expansion microchannel.
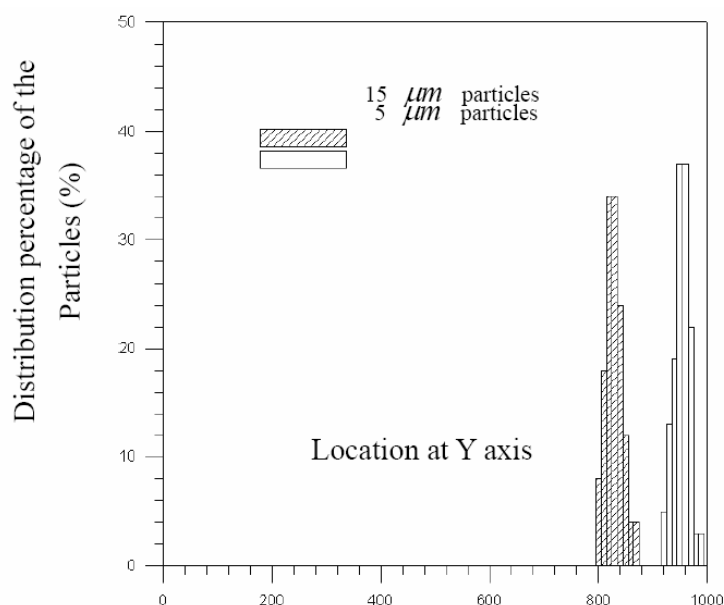
1742

Fig. 7. Location distribution percentage of 5 μm and 15 μm particles at Y-axis.

Fig. 7 indicates the location distribution ratios of the 5 μm and 15 μm particles from the bottom of the sidewall of the expansion channel when one hundred 5 μm particles and one hundred 15 μm particles are injected from Inlet 1. From the figure, it can be seen that about 37% of the 5 μm particles are distributed at a location 950 μm from the bottom sidewall. About 34% of the 15 μm particles are distributed at a location 830 μm from the bottom sidewall. The distance between the two different sized particles is approximately 120 μm. From Figs. 6 and 7, we can see that the device composed of the Y-shaped microchannel and the sudden expansion microchannel can accomplish a separation effect for different sizes of particles.
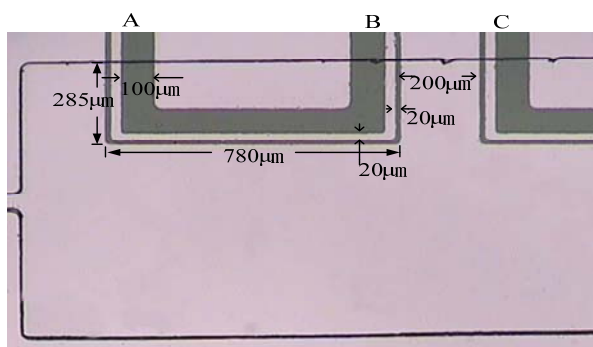

Fig. 8. Designed microelectrodes within the sudden expansion microchannel.

Fig. 8 shows the designed microelectrode patterns within the sudden expansion microchannel. Three pairs of U-shaped asymmetric microelectrodes are designed to be embedded on the substrate within the expansion channel. The width of the slim outer electrodes outside of the U-shaped microelectrodes is 20 μm, and the distance between the bottom side of the slim electrodes and the upper sidewall of the expansion channel is 285 μm, in order to ensure that 5 μm particles can move into the inside region of the U-shaped microelectrodes. The width of the wider interior electrodes is 100 μm, and the gap of the slim and wider electrodes is 20 μm. The distance between these three pairs of electrodes is 200 μm, respectively. The purpose of the designed U-shaped microelectrodes is mainly to make the 5 μm particles move smoothly into the U-shaped microelectrodes and become trapped within the region of the U-shaped microelectrodes. However, for particles of 15 μm, due to the trajectory of the particles outside of the region of the U-shaped microelectrodes, the particles could not be trapped by the electrodes and move downstream. Therefore, at

the outlet of the microchannel, the 15 μm particles could be collected. For particles of 5 μm, due to their original moving trajectories passing through the region of the U-shaped electrodes, the movement of the particles is affected by the induced AC electroosmotic flow of the asymmetric electrodes. As mentioned in Fig. 1, asymmetric electrodes induce different sized fluid rolls over each electrode, leading to a net fluid flow from narrow electrodes to wide electrodes. As shown schematically in Fig. 8, in the "A" region of the figure, the induced net fluid flow of the AC electroosmotic flow from narrow electrodes to wide electrodes makes the 5 μm particles move into the U-shaped electrodes. Contrarily, in the "B" region of the figure, the designed electrodes induce a reversed moving net flow which hinders the particles moving forward. Through the electrode design, the 5 μm particles can be trapped with the induced AC electroosmotic flow of the electrodes. In order to ensure that all of the injected 5 μm particles can be trapped, another two pairs of U-shaped electrodes were designed downstream. For the 15 μm particles, due to their trajectories outside of the U-shaped electrodes, they are not affected by the induced AC electroosmotic flow and move downstream with the inertia momentum. Thus, the 15 μm particles can be collected at the outlet of the Y-shaped microchannel.
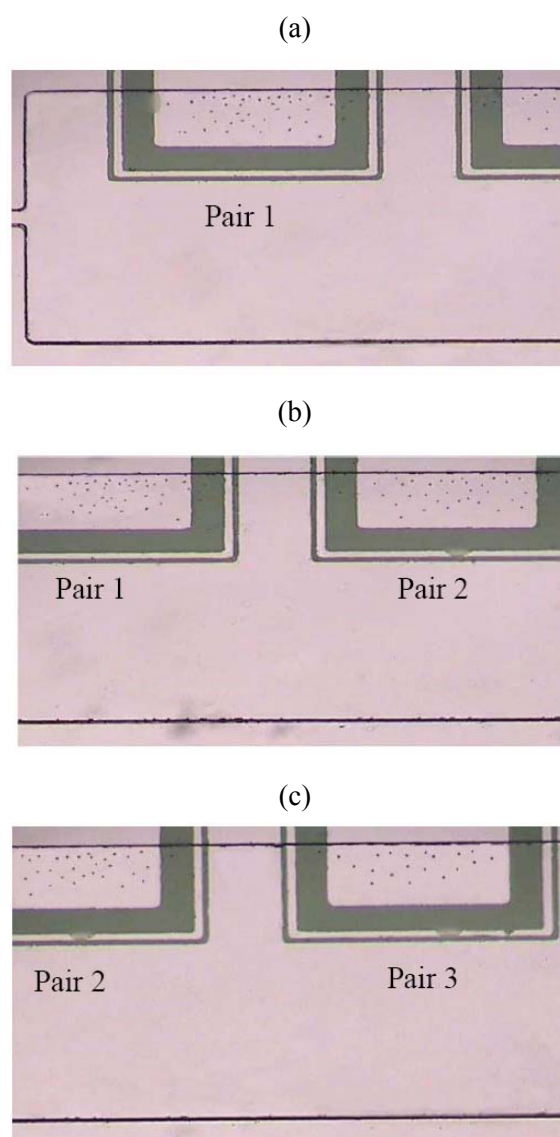
(a)

(b)

(c)

Fig. 9. Distribution of trapped particles within U-shaped microelectrodes.

Fig. 9 illustrates the distribution of 100 particles within the U-shaped electrodes to which an AC electric potential of 3 Vpp voltage and 2k Hz frequency was applied. For the one hundred particles, 43, 32 and 20 particles were trapped within the first, second and third pair of U-shaped electrodes,

respectively, as shown in Figs. 9(a), 9(b) and 9(c). Figure 10 shows the percentages of the trapped particles by the three pairs of U-shaped electrodes to which AC electric potentials of 3 Vpp at different frequencies were applied. In the case of the AC electric potential with a 2k frequency, 43%, 32% and 20% of the particles were trapped by the first, second and third pair of U-shaped electrodes, respectively. The amount of trapped particles decreases from the upstream electrode pair to the downstream electrode pair. Some of the particles whose trajectories near the upper wall are outside the region of the induced rolls on the electrodes are not affected by the induced AC electroosmotic flow. Thus, there were still 5% of the particles that were not trapped by the three pairs of electrodes.
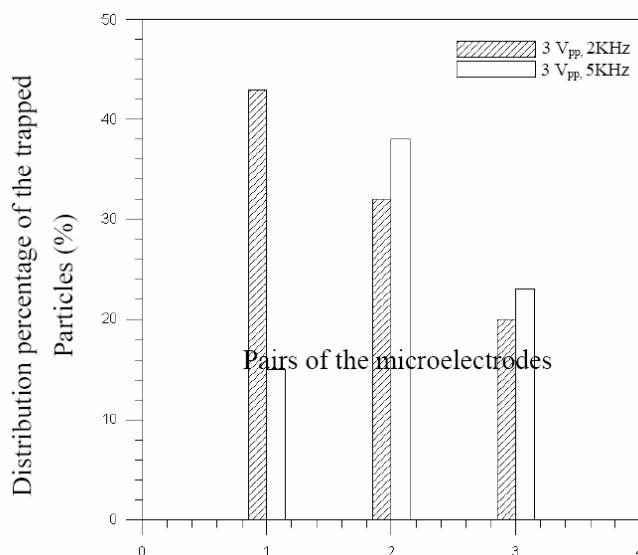

Fig. 10. Distribution percentage of trapped particles within the microelectrodes with AC electric potentials of 3 Vpp voltage, 2 KHz and 5 KHz frequency applied.

In the case of the AC electric potential with a 5 k frequency, 15%, 38% and 33% of the particles were trapped by the first, second and third pair of U-shaped electrodes, respectively. With the increase in the frequency of the applied AC potential, the pumping velocity of the induced electroosmotic flow moving from small electrodes to large electrodes is greater than that in the case with a low frequency of applied AC potential. Due to the larger pumping velocity, the amount of particles trapped by the first pair of U-shaped electrodes is the least among the three pairs of electrodes. The amount of particles trapped by the second pair of U-shaped electrodes is equivalent to that of the third pair of U-shaped electrodes. Moreover, a greater induced pumping velocity of the induced electroosmotic flow leads to an increase in particles' inertial momentum. However, since only three pairs of U-shaped electrodes were designed, some of the particles with greater moving momentum or whose trajectories near the upper wall were outside the region of the induced rolls on the electrodes were not trapped by the electrodes. In this case, 14% of the particles were still not trapped. It can be conjectured that with an increase in the amount of U-shaped electrodes, the percentage of trapped particles can be enhanced.

4. Conclusions

Currently, utilizing an AC electroosmotic flow for the separation and trapping of microparticles in a microchannel chip with microelectrodes is still novel research. It is essential to develop a thorough understanding of the evolution of these flow-field conditions when such a device is designed, and to compare it with other applications of microchannel chips for trapping particles; particle separation, such as the specific design of a geometric structure of the microchannel; and the manufacture of applied potentials. The designed Y-shaped microchannel with a pinched segment and sudden expansion channel accompanied with embedding asymmetric pairs of microelectrodes on a sudden expansion microchannel can generate a steadier recirculation region above the electrodes. When combining pressure with AC electric potential, designing additional particle trapping channels is unnecessary. One channel can accomplish the trapping of different sizes of particles at

the same time. Therefore, it can significantly shorten the dimension of the designed device during separation. Moreover, it is simpler for chip fabrication and design, and possesses better separation efficiency.

References

[1] J.C. Giddings, Science. **206**(5113), 1456 (1993).
[2] W.S. Kim, Y.H. Park, J.Y. Shin, D.W. Lee, S. Lee, Anal. Chem. **17**, 3265 (1999).
[3] W.J. Lee, B.R. Min, M.H. Moon, Anal. Chem. **71**, 3446 (1999).
[4] X.B. Wang, J. Yang, Y. Huang, J. Vykoukal, F.F. Becker, P.R.C. Gascoyne, Anal. Chem. **72**, 832 (2000).
[5] T.L. Edwards, B.K. Gale, A.B. Frazier, Anal. Chem. **74**, 1211 (2002).
[6] H.J. Small, Colloid Interface Sci. **48**, 147 (1974).
[7] A.W. Thronton, J.P. Oliver, C.G. Smart, L.B. Gilman, ACS Symp. Ser. **332**, 256 (1987).
[8] A. Williams, E. Verala, E. Mechan, K. Tribe, Int. J. Pharm. **242**, 295 (2002).
[9] E. Chmela, R. Tijssen, M.T. Blom, H.J.G.E. Gardeniers, A. van den Berg, Anal. Chem. **74**(14), 3470 (2002).
[10] C.A. Silebi, J.G. Dosramos, J. Colloid Interface Sci. **130**, 14 (1989).
[11] C.M. Miller, E.D. Sudol, C.A. Silebi, M.S. El-Aasser, J. Colloid Interface Sci. **172**, 249 (1995).
[12] J.C. Giddings, Sep. Sci. Technol. **20**, 749 (1985).
[13] Y. Jiang, A. Kummerow, M.J. Hansen, Microcolumn Sep. **9**, 261 (1997).
[14] F. Dondi, C. Contado, G. Blo, S.G. Martin, Chromatographia **48**, 643 (1998).
[15] C.B. Fuh, Anal. Chem. 72, 266A (2000).
[16] R.W. Applegate, J.J. Squier, T. Vestad, J. Oakey, D. Marr, Optics Express **12**, 4390 (2004).
[17] M.M. Wang, E.Tu.D.E. Raymond, J.M. Yang, H. Zhang, N. Hagen, B. Dees, E.M. Mercer, A.H. Forster, I. Kariv, P.J. Marchand, W.F. Butler, Nature Biotechnology **23**, 83 (2005).
[18] A.Y. Fu, C. Spence, A. Scherer, F.H. Arnold, S.R. Quake, Nature Biotechnology **17**, 1109 (1999).
[19] M.L. Plenert, J.B. Shear, Proceedings of the National Academy of Sciences **100**, 3853 (2003).
[20] M. Yamada, M. Nakashima, M. Seki, Anal. Chem. **76**, 5465 (2004).
[21] X. Xuan, C. Ye, D. Li, Journal of Colloid and Interface Science **289**, 286 (2005).
[22] X. Xuan, B. Xu, D. Li, Anal. Chem. **77**, 4323 (2005).
[23] X. Xuan, D. Li, Journal of Micromechanics and Microengineering **16**, 62 (2006).
[24] Y.Li.D. Kang, S.A. Kalams, J.E. Eid, Biomedical Microdevices **10**(2), 243 (2008).
[25] K.S. Chow, H. Du, Sensors and Actuators A **170**, 24 (2011).
[26] R. Zhang, J. Koplik, Physical Review E **85**(2), 026314 (2012).
[27] K. Khoshmanesh, S. Baratchi, F.J. Tovar-Lopez, S. Nahavandi, D. Wlodkowic, A. Mitchell, K. Kalantar-Zadeh, Microfluidics and Nanofluidics **12**(1-4), 597 (2012).
[28] M. Yamada, M. Seki, Anal. Chem. **78**(4),1357 (2006).
[29] N.G. Green, A. Ramos, A. Gonzalez, H. Morgan, A. Castellanos, Physical Review E **61**(4B), 4011 (2000).
[30] A. González, A. Ramos, A., N.G. Green, A. Castellanos, A., H. Morgan, Physical Review E **61**(4B), 4019 (2000).
[31] N.G. Green, A. Ramos, A. Gonzalez, H. Morgan, and A. Castellanos, Physical Review E **66**(2), 026305 (2002).
[32] J.K. Chen, W.J. Luo, R.J. Yang, Japanese Journal of Applied Physics **45**(10A), 7983 (2006).
[33] W.J. Luo, K.F. Yarn, S.P. Hsu, Japanese Journal of Applied Physics **46**(4A), **1608** (2007).
[34] W.J. Luo, Microfluidics and Nanofluidics **6**(2), 189 (2009).